2010

Reconstruction from limited-angle projections based on spectrum analysis

Jianhua Luo
Shanghai Jiao Tong University

Wanqing Li
University of Wollongong, wanqing@uow.edu.au

Yuemin Zhu
University of Lyon

Reconstruction from limited-angle projections based on spectrum analysis

Abstract

This paper proposes a sparse representation of an image using discrete δ-*u* functions. A δ-*u* function is defined as the product of a Kronecker delta function and a step function. Based on the sparse representation, we have developed a novel and effective method for reconstructing an image from limited-angle projections. The method first estimates the parameters of the sparse representation from the incomplete projection data, and then directly calculates the image to be reconstructed. Experiments have shown that the proposed method can effectively recover the missing data and reconstruct images more accurately than the total-variation (TV) regularized reconstruction method.

Disciplines

Physical Sciences and Mathematics

Publication Details

Luo, J., Li, W. & Zhu, Y. (2010). Reconstruction from limited-angle projections based on spectrum analysis. IEEE Transactions on Image Processing, 19 (1), 131-140.

Reconstruction From Limited-Angle Projections Based on $\delta - u$ Spectrum Analysis

Jianhua Luo, Wanqing Li, *Member, IEEE*, and Yuemin Zhu

***Abstract*—This paper proposes a sparse representation of an image using discrete $\delta - u$ functions. A $\delta - u$ function is defined as the product of a Kronecker delta function and a step function. Based on the sparse representation, we have developed a novel and effective method for reconstructing an image from limited-angle projections. The method first estimates the parameters of the sparse representation from the incomplete projection data, and then directly calculates the image to be reconstructed. Experiments have shown that the proposed method can effectively recover the missing data and reconstruct images more accurately than the total-variation (TV) regularized reconstruction method.**

***Index Terms*—Limited angle, sparse representation, tomography, $\delta - u$ function, $\delta - u$ spectrum analysis.**

I. Introduction

THE aim of computerized tomography (CT) is to reconstruct the image of an unknown physical object from a collection of projections. The quality of the reconstructed image depends on many factors including the range of the projection angles and the noise level of the projection data. According to CT theory [1], an image can be reconstructed exactly from complete projections covering a full angular range of 180°. However, such a complete projection data may be hard to obtain in some cases due to the practical constraints imposed on the object or imaging environment. In such cases, projections can only be acquired from a limited range of angles. For instance, an object to be inspected may be too big to fit into an X-ray CT scanner. As a result, the feasible projection angle ϕ is limited to a small range $\phi \in [\phi_1, \phi_2]$, where $0 < \phi_1 < \phi_2 < \pi$, as shown in Fig. 1(d). Although the angular sampling within the limited range and the sampling of each projection can be sufficiently dense, the projection data is incomplete [1]–[4]. This paper addresses the problem of reconstructing images from limited-angle projections.

In the past decades, the problem of image reconstruction from projection data, especially from limited-angle projections, has been actively studied. Loosely speaking, image reconstruction methods can be divided into three categories [1], [5], [6]: analytical, iterative, and statistical. Analytical methods derive the exact image reconstruction formula from the imaging physics and geometry. A typical example is the widely used filtered backprojection (FBP) method [1] which is based on the Radon transform and Fourier slice theorem. Reconstruction based on other transforms, such as the finite Hilbert transform [7], has also been explored. Analytical methods often offer efficient and effective reconstruction when the projection data is complete. In the case of limited-angle projections, existing analytical methods usually produce severe artifacts in the reconstructed image because of their inability to deal with incomplete data. Recently, Kesidis and Papamarkos [6] proposed a method for exact image reconstruction from a limited number of projections. The method is useful in image analysis as demonstrated in [6], but would be infeasible for limited-angle CT due to the requirements on the projection directions. Tomitani and Hirasawa [8], [9] proposed an analytical method for image reconstruction of cone-beam projections from limited-angle Compton camera data. The method is based on an inversion of the summed projections and sacrifices the spatial resolution for noise suppression.

Iterative methods consider the reconstruction problem as a discrete linear system where projection data is a weighted sum over the image pixels (or voxels) and solve the linear system by optimizing a linear or nonlinear objective function [1], [10]. A typical solution is the algebraic reconstruction technique (ART) [1], [5], [11], [12] in which the reconstruction is accomplished by iteratively updating the estimation of the reconstructed image so that the error between the measured and calculated projection data is minimized. The basic ART updates the reconstructed image in a "ray-by-ray" manner and converges to a least squared error solution that can be very noisy for limited-angle reconstruction [11]. Various improvements have been introduced to the ART depending on the amount of projection data and the way used to update the current estimation [1], [5]. In the case of limited-angle projections, the reconstruction problem becomes ill-posed and to solve the linear system, additional constraints such as non-negativity of pixel values, piecewise smoothness and prior information about the reconstructed image are required. These constraints are usually introduced to the objective function as a term of regularization [5], [10], [13]–[16]. For instance, Sidky and Pan [13], [14] proposed an iterative method for circular cone-beam

Manuscript received January 07, 2009; revised August 27, 2009. First published September 22, 2009; current version published December 16, 2009. This work was supported in part by the NSF of China under 30670574, in part by the project Mira Recherche 2008 of the Region Rhône-Alpes of France, in part by the Shanghai International Cooperation Grant under 06SR07109, in part by the joint project of Chinese NSFC and French ANR 2009, and in part by the High Technology Research Development Plan (863 plan) of China under 2006AA020805. The associate editor coordinating the review of this manuscript and approving it for publication was Prof. Minh N. Do.

J. Luo is with the College of Life Science and Technology, Shanghai Jiao Tong University, 200240, Shanghai, China (e-mail: jhluo@sjtu.edu.cn).

W. Li is with the School of Computer Science and Software Engineering, University of Wollongong, NSW 2522, Australia (e-mail: wanqing@uow.edu.au).

Y. Zhu is with CREATIS, CNRS UMR 5220, Inserm U 630, INSA Lyon, University of Lyon 1, University of Lyon, Lyon, France (e-mail: yue-min.zhu@creatis.insa-lyon.fr).

Color versions of one or more of the figures in this paper are available online at http://ieeexplore.ieee.org.

Digital Object Identifier 10.1109/TIP.2009.2032893

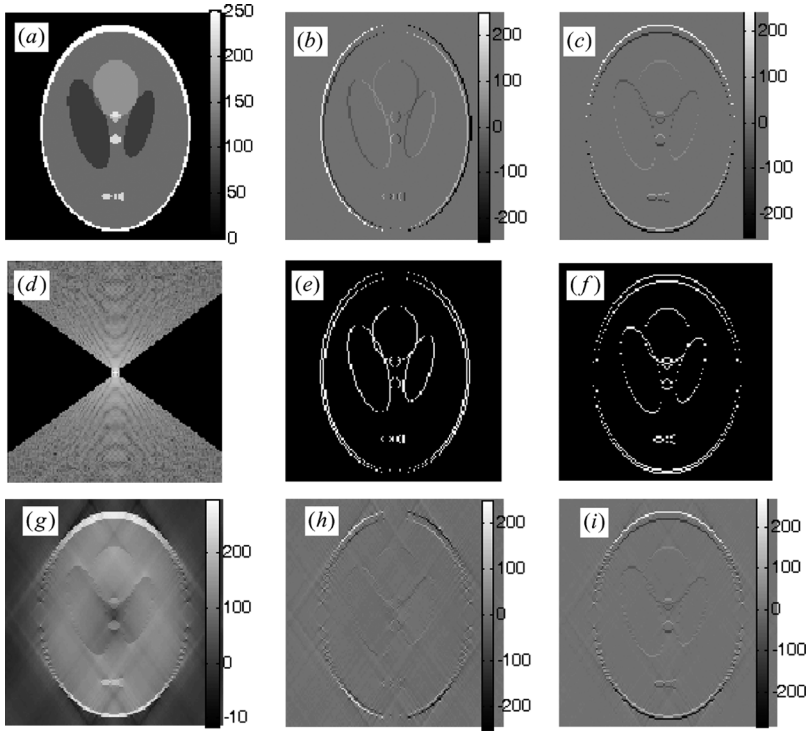

Fig. 1. (a) Reference image. (b) and (c) are respectively $\Delta_y f(x, y)$ and $\Delta_x f(x, y)$. (d) Spectrum $\lg(1+|F(k_x, k_y)|)$. (e) and (f) represent the images of singular points derived respectively from (b) and (c). (g) $\bar{f}(x, y)$ reconstructed from the zero-padded limited-angle spectral data (11). (h) and (i) represent $\Delta_y \bar{f}(x, y)$ and $\Delta_x \bar{f}(x, y)$ of $\bar{f}(x, y)$, respectively.

CT by minimizing the total variation of the image subject to the constraints that the estimated projection data is within a specific tolerance of the available data, and that the image is non-negative. In [5], constraints are derived from the desired properties of the reconstructed binary image by ensuring that the changes in the contour are restricted to the solutions of the level set function modeling the distribution of the binary contours.

In statistical methods [17]–[19], pixel (or voxel in 3-D cases) values of the reconstructed image are considered as random variables following some probability distribution. For instance, the distribution is represented as a wavelet expansion and a Besov space prior distribution is assumed in [18]. In [19], the distribution is obtained from previous sample data of the same patient. Statistical methods explicitly take into account the measurement statistics and noise model. They reconstruct the image by searching for pixel values such that the measured data has the largest probability of occurrence, that is, maximum likelihood (ML) solution. Due to the fact that there is no analytical way to find an ML solution, algorithms such as the expectation-maximization (EM), convex algorithms and gradient algorithms are often used to find the solution in an iterative manner.

The major advantage of the iterative and statistical methods is that they do not assume the completeness of the projection data. However, they all suffer from a number of problems that are inherent in any iterative approach. First, they are highly sensitive to the initial values of the estimated image and iterative parameters such as the step size and relaxation parameter in ART. Different initial values could lead to the reconstructed images having substantially different image quality. Second, appropriate stopping criterion of the iterative process has to be chosen and the choice of the criterion affects the quality of the reconstructed image. Third, they hardly converge to a global optimal solution. Finally, they are often very time-consuming compared with analytical methods. Some details on different methods of reconstruction from limited-angle projections can be found in recent review articles [20], [21].

This paper proposes a novel and effective method for reconstructing images from limited-angle projections. Like classical analytical methods, the method reconstructs images using an analytical expression. However, unlike the classical ones that reconstruct images directly from projection data using the analytical inversion formula, the method does not reconstruct images directly from projection data, but from a sparse representation of an image using discrete $\delta-u$ functions, each being defined as the product of a Kronecker delta function and a step function. The parameters of the sparse representation are estimated from the limited projection data. The major advantages of the proposed method are that it can effectively recover missing data without any prior knowledge and it does not suffer from the problems that iterative and statistical methods have.

The rest of the paper is organized as follows. Section II defines the discrete $\delta - u$ functions and proposes the sparse representation of images using the functions. The spectral analysis of the $\delta - u$ functions is described. In Section III, the image reconstruction method for limited-angle projections is derived from the $\delta - u$ representation. A layered algorithm is proposed for estimating the parameters of the sparse representation from the limited projection data. Experimental results and analysis are given in Section IV and Section V concludes the paper with remarks.

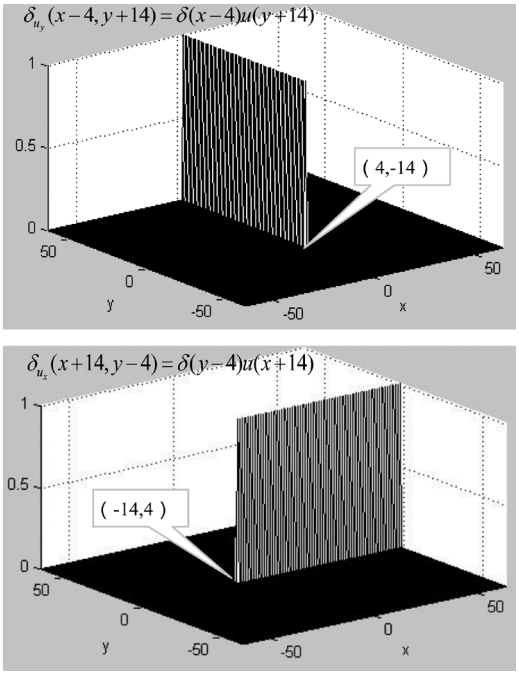

Fig. 2. Illustration of $\delta-u$ functions. $\delta_{u_y}(x+14,y-4)=\delta(x+14)u(y-4)$ (upper row) and $\delta_{u_x}(x+14,y-4)=u(x+14)\delta(y-4)$ (lower row).

II. Image Representation Using $\delta - u$ Functions

This section introduces discrete $\delta-u$ functions and the sparse representation of an image using these functions. The spectral analysis of the $\delta - u$ functions is also presented.

A. Definition of Discrete $\delta - u$ Functions

Let (x, y) be a point in a 2-D Cartesian lattice L. A discrete $\delta - u$ function on L, denoted as $\delta_u(x-a, y-b)$, is defined as the product of a Kronecker delta function (simply referred to as a delta function hereafter) in one dimension and a unit step function in another dimension, where $a, b \in \mathrm{Z}$ are the parameters of the $\delta - u$ function. Depending on the selection of the dimension for the delta function and the step function respectively, $\delta_u(x-a, y-b)$ can be written either as

$$\delta_{u_y}(x-a, y-b) = \delta(x-a)u(y-b) \tag{1}$$

where $\delta(x-a) = \begin{cases} 1, & x=a \\ 0, & x \neq a \end{cases}$ and $u(y-b) = \begin{cases} 1, & y \geq b \\ 0, & y < b \end{cases}$ or as

$$\delta_{u_x}(x-a, y-b) = \delta(y-b)u(x-a) \tag{2}$$

where $\delta(y-b) = \begin{cases} 1, & y=b \\ 0, & y \neq b \end{cases}$ and $u(x-a) = \begin{cases} 1, & x \geq a \\ 0, & x < x \end{cases}$.

Fig. 2 illustrates two examples of the $\delta-u$ function (on a 128×128 Cartesian lattice): $\delta_{u_y}(x+14, y-4) = \delta(x+14)u(y-4)$ and $\delta_{u_x}(x+14, y-4) = u(x+14)\delta(y-4)$.

B. Sparse Representation of an Image Using $\delta - u$ Functions

A discrete image $f(x, y)$ can be considered as a discrete function defined on a 2-D finite Cartesian lattice L. Without loss of generality, we assume that the image has $N * N = N^2$ pixels, that is, $x = 1, 2, \cdots, N$ and $y = 1, 2, \cdots, N$. $f(x, y)$ can then be expressed as

$$f(x,y) = \sum_{i=1}^{N}\sum_{j=1}^{N} a_{ij}\delta(x-i, y-j), \quad 1 \leq x, y \leq N \tag{3}$$

where a_{ij} represents the pixel value at (i, j) and $\delta(x-i, y-j)$ is a 2-D delta function.

Using the $\delta - u$ functions, we can rewrite (3) as

$$f(x,y) = \sum_{q=1}^{Q} a_q \delta_u(x-x_q, y-y_q), \quad 1 \leq x, y \leq N \tag{4}$$

where the parameters $(x_1, y_1), (x_2, y_2), \ldots, (x_Q, y_Q)$ of the $\delta - u$ functions are referred to as singular points of image $f(x, y)$, Q is the number of singular points, and the weighting coefficients $\{a_1, a_2, \ldots, a_Q\}$ are called as the singular degrees corresponding to the singular points.

Equation (4) is a rather universal representation of discrete images, which allows us to represent not only piecewise constant images, but also any other types of images, the only difference being in the number of used $\delta - u$ functions. For instance, in the case that the image is purely composed of noise, each pixel of the image is a singular point, and the number of singular points is equal to the number of image pixels, that is, $Q = N^2$. In most cases, an image always presents some spatial correlation. As a result, we have in general $Q \ll N^2$, and the number of independent variables would be significantly reduced when reconstructing or representing the image. Therefore, (4) actually becomes a sparse representation of the image $f(x, y)$. If the image $f(x, y)$ is spatially piecewise constant, that is, the image is composed of spatially correlated segments and pixels in each segment share the same value, the sparsity becomes particularly high. This is often the case for medical X-ray CT images and industrial and security X-ray scanning since the X-ray attenuation coefficient often varies little within the same tissues and materials. In fact, the piecewise constant assumption is also the key assumption employed in all TV-based reconstruction methods [13], [14].

Substituting (1) or (2) in (4) yields

$$f(x,y) = \sum_{q=1}^{Q} a_q \delta_{u_y}(x-x_q, y-y_q) \quad 1 \leq x, y \leq N \tag{5}$$

$$f(x,y) = \sum_{q=1}^{Q} a_q \delta_{u_x}(x-x_q, y-y_q) \quad 1 \leq x, y \leq N. \tag{6}$$

For a given image, (5) and (6) can be obtained respectively by scanning the image in a column-by-column or row-by-row manner. For example, assume that the values of the first 9 pixels in the j*'th* row of an image is 1,1,1,2,2,2,0,0,0. These pixel values can be represented using the $\delta - u$ functions as $\delta(y-j)(u(x-1)+u(x-4)-2u(x-7))$, where $\delta(y-j)$ selects the jth row and $(u(x-1)+u(x-4)-2u(x-7))$ represents the pixel values.

Let us consider the difference between two neighboring pixels in the same column (along the vertical y-direction). From (5) and (1), we have

$$\Delta_y f(x,y) = f(x,y) - f(x,y-1) = \sum_{q=1}^{Q} a_q \delta(x - x_q, y - y_q), \quad 1 \le x, y \le N. \quad (7)$$

Equation (7) reveals that singular points are located at the pixels whose difference value along the y-direction is not zero. Similarly, singular points are located at the pixels whose difference along x-direction is not zero if the image is represented as (6).

C. $\delta - u$ Spectral Analysis of Images

Let $F(k_x, k_y) = DFT[f(x,y)]$ be the Fourier spectrum of $f(x,y)$ and $U_q(k_x, k_y) = DFT[\delta_{u_y}(x - x_q, y - y_q)]$ be the Fourier spectrum of the $\delta - u$ function. Taking discrete Fourier transform of both sides of (5) leads to

$$F(k_x, k_y) = \sum_{q=1}^{Q} a_q U_q(k_x, k_y), \quad 1 \le k_x, k_y \le N. \quad (8)$$

Equation (8) indicates that the Fourier spectrum of the image is a weighed sum of the spectra of the $\delta - u$ functions. We refer to (8) as the $\delta - u$ spectral analysis of image $f(x,y)$. Similar spectrum analysis formula can be derived from (6).

Equations (5) and (8) define a general model of $\delta - u$ analysis of images, with which, for a given set of $\delta - u$ functions (or $\delta - u$ spectrum functions), any image and its spectrum can be completely determined solely by its singular points and the corresponding singular degrees or weighting coefficients. In addition, an image can be expressed in terms of two different sets of singular points corresponding to the choice of (5) or (6). The number and locations of the singular points in the two sets are often different depending on the structure of the image. For the given image shown in Fig. 1(a), there are 730 singular points [as shown in Fig. 1(e)] and, therefore, 730 $\delta - u$ functions are required to represent the image using $\delta_{u_y}(x - x_q, y - y_q)$ whereas only 525 $\delta - u$ functions are required when $\delta_{u_x}(x - x_q, y - y_q)$ is adopted. In the case that the singular points of image $f(x,y)$ are known, only small proportion of the spectral data of $f(x,y)$ is required to determine the weighting coefficients. Therefore, the $\delta - u$ sparse representation of an image provides an effective way to recover missing data. In the following section, we will describe our method to reconstruct an image from limited-angle projections through $\delta - u$ spectrum analysis.

III. Limited-Angle Image Reconstruction Using $\delta - u$ Spectrum Analysis

According to the Radon transform and Fourier slice theorem [1], [5], [6], the 1-D Fourier transform of the data projected from one direction is a slice of the 2-D Fourier transform of the image. The slice goes through the origin of the 2-D spectral space and is perpendicular to the direction of the projection. In the case of complete projections that continuously scan over 180°, the slices from all projection directions constitute a complete Fourier spectrum of the image to be reconstructed. In limited-angle projections, the projections are limited to certain range of angles and the spectral slices acquired from the projections only form a partial or incomplete spectrum of the image to be reconstructed [as shown in Fig. 1(d)]. The partial spectral data is known as limited-angle spectral data and the scanned spectral space having spectral data is referred to as limited-angle space. The missing spectral data needs to be recovered so as to reconstruct the image.

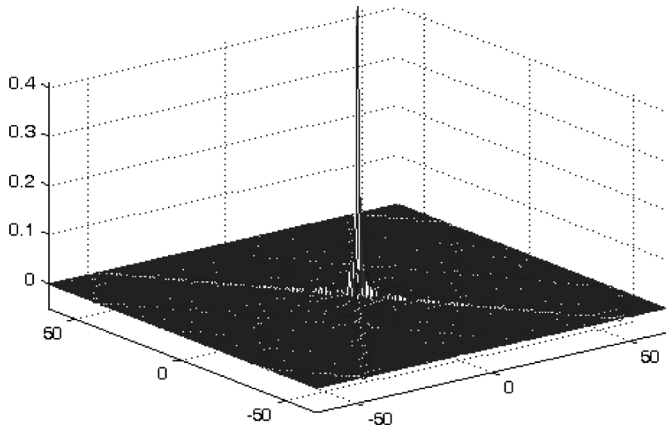

Fig. 3. Degraded delta function $i(x,y)$.

Let $I(k_x, k_y)$ be a binary mask matrix defined in the spectral space of the image to be reconstructed and elements are ones if they are within the limited-angle space and zeroes otherwise. That is

$$I(k_x, k_y) = \begin{cases} 1, & \text{arctg}(k_y/k_x) \in \text{limited} - \text{angle space} \\ 0, & \text{otherwise.} \end{cases} \quad (9)$$

For complete projections, all elements of $I(k_x, k_y)$ will be ones. We then have $\|I(k_x, k_y)\| = N^2$, where $\|I(k_x, k_y)\|$ denotes the number of nonzero elements in $I(k_x, k_y)$, and the inverse Fourier transform of $I(k_x, k_y)$ will be a delta function. In the case of limited-angle projections, let

$$i(x,y) = IDFT\,[I(k_x, k_y)] \quad (10)$$

where IDFT designates inverse discrete Fourier transform, be the degraded delta function (Fig. 3), due to the missing spectral data outside the limited-angle space. Since $I(k_x, k_y)$ is always symmetric to the origin, $i(x,y)$ is a real function.

$F(k_x, k_y)$ being the Fourier spectrum of the image $f(x,y)$, $F(k_x, k_y) \cdot I(k_x, k_y)$ is the spectrum obtained from the limited-angle projections with zeros padding to the elements outside the range of the projection angles. If the image $\tilde{f}(x,y) = IDFT(F(k_x, k_y) \cdot I(k_x, k_y))$ contains sufficient information on the singular points of $f(x,y)$, we can estimate the singular points and their singular degrees respectively from $\tilde{f}(x,y)$ and $F(k_x, k_y) \cdot I(k_x, k_y)$ and then reconstruct the original image $f(x,y)$ using its $\delta - u$ representation [equation (5) or (6)]. $\tilde{f}(x,y)$ is a degraded version of $f(x,y)$ given by

$$\tilde{f}(x,y) = IDFT\,[F(k_x, k_y) I(k_x, k_y)] = f(x,y) * i(x,y) \quad (11)$$

where $*$ denotes convolution.

A. Extraction of Singular Points

Notice from (11) that the degradation of the reconstructed image resulted from the limited-angle projections is equivalent to the convolution of the original image with the degraded delta function $i(x,y)$, as shown in Fig. 1(g). Similarly, the difference image along the y-direction has also been corrupted by the degraded function $i(x,y)$

$$\begin{aligned}\Delta_y\tilde{f}(x,y) &= \tilde{f}(x,y) - \tilde{f}(x,y-1)\\ &= f(x,y) * i(x,y) - f(x,y-1) * i(x,y)\\ &= \Delta_y f(x,y) * i(x,y). \end{aligned} \tag{12}$$

Substituting (7) into (12), we have

$$\begin{aligned}\Delta_y\tilde{f}(x,y) &= \sum_{q=1}^{Q} a_q \delta(x-x_q, y-y_q) * i(x,y)\\ &= \sum_{q=1}^{Q} a_q i(x-x_q, y-y_q) \end{aligned} \tag{13}$$

where $i(x-x_q, y-y_q)$ is the function $i(x,y)$ being shifted to the singular point (x_q, y_q).

Comparing (13) to (7), it can be seen that the difference in the limited-angle projections case has become the weighted sum of the functions $i(x-x_q, y-y_q)$ instead of delta functions $\delta(x-x_q, y-y_q)$, but the weighting coefficients remain unchanged. Notice that $\delta(x-x_q, y-y_q)$ is zero everywhere except at the location of (x_q, y_q) whereas $i(x,y)$ has nonzero values at almost all locations. This means that it is impossible to detect the singular points from the difference image $\Delta_y\tilde{f}(x,y)$ simply using nonzero difference values. Fig. 1(b) and (h) clearly shows respectively the $\Delta_y f(x,y)$ and $\Delta_y\tilde{f}(x,y)$ of the Shepp–Logan phantom, and Fig. 1(c) and (i) demonstrate the $\Delta_x f(x,y)$ and $\Delta_x\tilde{f}(x,y)$. Both $\Delta_x\tilde{f}(x,y)$ and $\Delta_y\tilde{f}(x,y)$ have nonzero values at almost all pixels. The number of singular points that could have been detected from $\Delta_x\tilde{f}(x,y)$ or $\Delta_y\tilde{f}(x,y)$ is much larger than the number of true ones detected from $\Delta_x f(x,y)$ (525 points) or $\Delta_y f(x,y)$ (730 points) respectively.

According to (13), the difference image $\Delta_y\tilde{f}(x,y)$ is the superposition of Q oscillating functions $a_q i(x-x_q, y-y_q)$ centered at $(x_1,y_1), (x_2,y_2), \ldots$, and (x_Q, y_Q), respectively. All oscillating functions $a_q i(x-x_q, y-y_q)$ will interfere with each other. Singular points having higher singular degrees will have larger oscillations and stronger interference with the singular points having smaller singular degrees. When the largest oscillating component is removed from $\Delta_y\tilde{f}(x,y)$, the second largest oscillating component, which may be buried by the largest oscillating component, will become the largest. This leads us to extract the singular points from $\Delta_y\tilde{f}(x,y)$ in a layered manner. Assuming that the singular points are rearranged according to the absolute value of their singular degrees, that is, $(x_q,y_q), |a_q| > |a_{q+1}|, q = 1,2,\ldots,Q$, we have $|\Delta_y\tilde{f}(x_1,y_1)| = \max_{x,y\in\{1,2,\ldots,N\}}\{|\Delta_y\tilde{f}(x,y)|\}$ (i.e., $|\Delta_y\tilde{f}(x,y)|$ reaches the maximum value at the first singular point). Therefore, the point having the maximum $|\Delta_y\tilde{f}(x,y)|$ value is taken as the first singular point (x_1,y_1). Once the first singular point is detected, the component $\alpha \cdot i(x-x_1, y-y_1)$ corresponding to the first singular point, where $\alpha = \Delta_y\tilde{f}(x_1,y_1)\|I(k_x,k_y)\|/N^2$, is subtracted from $\Delta_y\tilde{f}(x,y)$, yielding the residue $\Delta_y\tilde{f}(x,y) - \alpha \cdot i(x-x_1, y-y_1)$. The point at which the absolute value of this residual image reaches maximum is then taken as the second singular point. Repeating this two-stage process until the maximum absolute value of the residue is smaller than a predefined threshold T, the Q singular points can be detected one by one.

Selection of the threshold T is subject to the noise level in the image. If it is too large, there is a risk of having false negative detection of the singular points. If it is too small, false positives are likely to occur due to the noise. Therefore, there exists an optimal value for the threshold T. Empirically, the optimal T value is around the value of four times the standard deviation of the noise; experimental results on the influence of the threshold T on the reconstruction are given in Section IV. The algorithm is described as follows.

Input: $\Delta_y^l\tilde{f}(x,y) = \Delta_y\tilde{f}(x,y)$ (or $\Delta_x\tilde{f}(x,y)$), $l = 0$.

Step 1) Find the location (x_q, y_q) at which $|\Delta_y^l\tilde{f}(x,y)|$ is maximum, i.e., $\max_{1\le x,y\le N}\{|\Delta_y^l\tilde{f}(x,y)|\}$.

Step 2) Construct the function $\alpha \cdot i(x-x_q, y-y_q)$ with $\alpha = \Delta_y\tilde{f}(x_q,y_q)\|I(k_x,k_y)\|/N^2$ Update $\Delta_y\tilde{f}(x,y)$ by subtracting $\alpha \cdot i(x-x_q, y-y_q)$ from it

$$\Delta_y^{l+1}\tilde{f}(x,y) = \Delta_y^l\tilde{f}(x,y) - \alpha \cdot i(x-x_q, y-y_q), \quad 1 \le x,y \le N. \tag{14}$$

Step 3) If $\max_{1\le x,y\le N}(|\Delta_y^{l+1}\tilde{f}(x,y)|) > T$, where T is a predefined threshold, $l = l+1$ and go to step 1 to extract the next singular point.

Step 4) Output the set of singular point candidates $\{(x_1,y_1),(x_2,y_2),\ldots,(x_P,y_P)\}$. After the singular points are obtained from $\Delta_y\tilde{f}(x,y)$, their singular degrees will be computed in the spectral domain as described in the following section.

B. Estimation of Singular Degrees

The singular degrees $\{a_1, a_2, \ldots, a_P\}$ corresponding to the detected singular points can be estimated by solving a set of linear equations formed by the obtained limited-angle spectral data and the $\delta - u$ spectra $U_q(k_x,k_y), q = 1,2,\ldots,P$ according to (8). The algorithm for determining singular points as well as singular degrees is given below.

Step 1) Calculate the Fourier spectrum of the limited-angle projections and construct the degraded function $i(x,y)$.

Step 2) Compute $\tilde{f}(x,y) = IDFT(F(k_x,k_y)\cdot I(k_x,k_y))$ and $\Delta_y\tilde{f}(x,y) = \tilde{f}(x,y) - \tilde{f}(x,y-1)$.

Step 3) Extract the singular point set $\{(x_1,y_1),(x_2,y_2),\ldots,(x_P,y_P)\}$ using the algorithm of layered singular points extraction.

Step 4) For each singular point (x_q,y_q), construct a $\delta - u$ function $\delta_{u_y}(x-x_q, y-y_q)$ (or $\delta_{u_x}(x-x_q, y-y_q)$) and calculate its spectrum

$$U_q(k_x,k_y) = DFT\left[\delta_{u_y}(x-x_q, y-y_q)\right], \quad q = 1,2,\ldots,P.$$

Step 5) From the limited-angle spectral data, construct a set of linear equations

$$F(k_x, k_y) = \sum_{q=1}^{P} a_q U_q(k_x, k_y) \tag{15}$$

with $arctg(k_y/k_x) \in$ limited−angle space.

Step 6) Estimate the singular degrees $\{a_1, a_2, \ldots, a_P\}$ by solving the linear system (15). If $a_q = 0$, then the q'th singular point is considered to be a false one and discarded therefore.

Note that solving the system of equations in spectral space aims at obtaining the singular degrees. When the true singular points are included in the set of singular point candidates detected using the layered extraction method, the nonzero solutions correspond to the true singular points, and the solutions that are equal to zero correspond to false singular points that will be discarded. If there are too many false singular points, the efficiency of solving the system of equations will be reduced, and moreover it would require more spectral data. On the other hand, if the set of detected singular point candidates contains only a subset of true singular points, the number of equations of the system is reduced, and the time of computation is reduced as well, but the solutions obtained in this case undergo errors.

In practical cases, images being always noisy, the singular points buried in the noise (i.e., singular points whose singular degrees are smaller than the noise level) are difficult to detect, and the determination of other singular points and their singular degrees are also subject to the influence of noise. Nevertheless, the missing singular points should yield relatively small reconstruction errors because they have small singular degrees due to the mechanism of the layered extraction. For these reasons the proposed method is resilient to noise as demonstrated in Section IV.

C. Reconstruction of $f(x, y)$

Given the estimated singular points and degrees, the image $f(x, y)$ can be directly calculated from the set of $\delta - u$ functions based on (4). Alternatively, the full spectrum $F(k_x, k_y)$ of the image is first estimated using (8) and $f(x, y)$ is calculated through inverse Fourier transform. Both methods are equivalent.

IV. Experimental Results

A. Experimental Setup

The popular Shepp–Logan phantom and real X-CT lung images were used to verify the theory of the $\delta - u$ spectrum analysis and effectiveness of the proposed method for image reconstruction from limited-angle projections, both of them have 256 × 256 pixels and 256 grey levels. Parallel projection in each direction consists of 363 data points, and angular sampling is uniform with the interval of 0.5°. Limited-angle projections were simulated by taking the projection data within the specified range of projection angles. Images were reconstructed using both the $\delta - u$ method and the TV method proposed in [14] and were compared with reference images. The TV method consists of the following steps: a) initialize the image to be reconstructed to zero; b) iteratively reconstruct the image such that its projections are consistent with the measured projections; c) impose the positivity constraint on the reconstructed image; d) update the reconstructed image iteratively using the gradient descent method to minimize its TV; e) repeat steps b), c) and d) until there is no appreciable change in the intermediate images. For the proposed $\delta - u$ method, the threshold T in all experiments was empirically set to 4σ where σ is the standard deviation of the noise in the image.

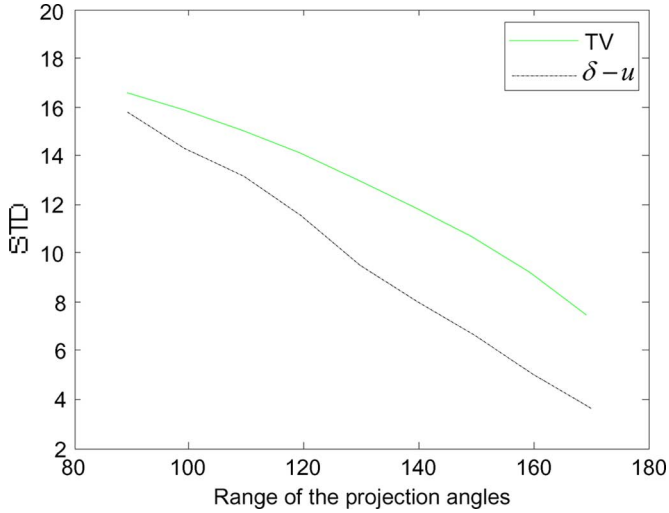

Fig. 4. STD values of the TV method and the proposed method with different ranges of the projection angles.

Both visual and objective comparisons were conducted. Visual comparison was made in both spatial and spectral (displayed as $\lg(1 + |DFT[f(x, y)]|)$ domains. To measure the accuracy of the reconstruction, we compute the standard deviation (STD) of the errors between the reconstructed image $f(x, y)$ and reference image $f_0(x, y)$

$$STD = \sqrt{\frac{1}{N^2} \sum_{x=1}^{N} \sum_{y=1}^{N} [e(x, y) - \bar{e}]^2} \tag{16}$$

where $e(x, y) = f(x, y) - f_0(x, y)$ and $\bar{e} = (1/N^2) \sum_{x=1}^{N} \sum_{y=1}^{N} e(x, y)$, and the peak signal-to-noise ratio (PSNR) of the reconstructed image

$$\mathrm{PSNR(dB)} = 10 \log_{10} \left(255^2 \Big/ \frac{1}{N^2} \sum_{x=1}^{N} \sum_{y=1}^{N} [e(x, y)]^2 \right). \tag{17}$$

B. Experimental Results

We first conducted a series of experiments to evaluate the reconstruction accuracy of the proposed method for different ranges of projection angles. Gaussian noise was added to the projection data such that the SNR of the projection data is about 29.8 dB. Images were reconstructed using the TV method and the proposed $\delta - u$ method by varying the projection angle range from 90° to 179°. The STD values for both methods are shown in Fig. 4.

The STD values have indicated that the proposed method significantly reduced the reconstruction errors and constantly outperformed the TV method for different ranges of projection angles. When the projection angle range is 144°, the PSNR of the

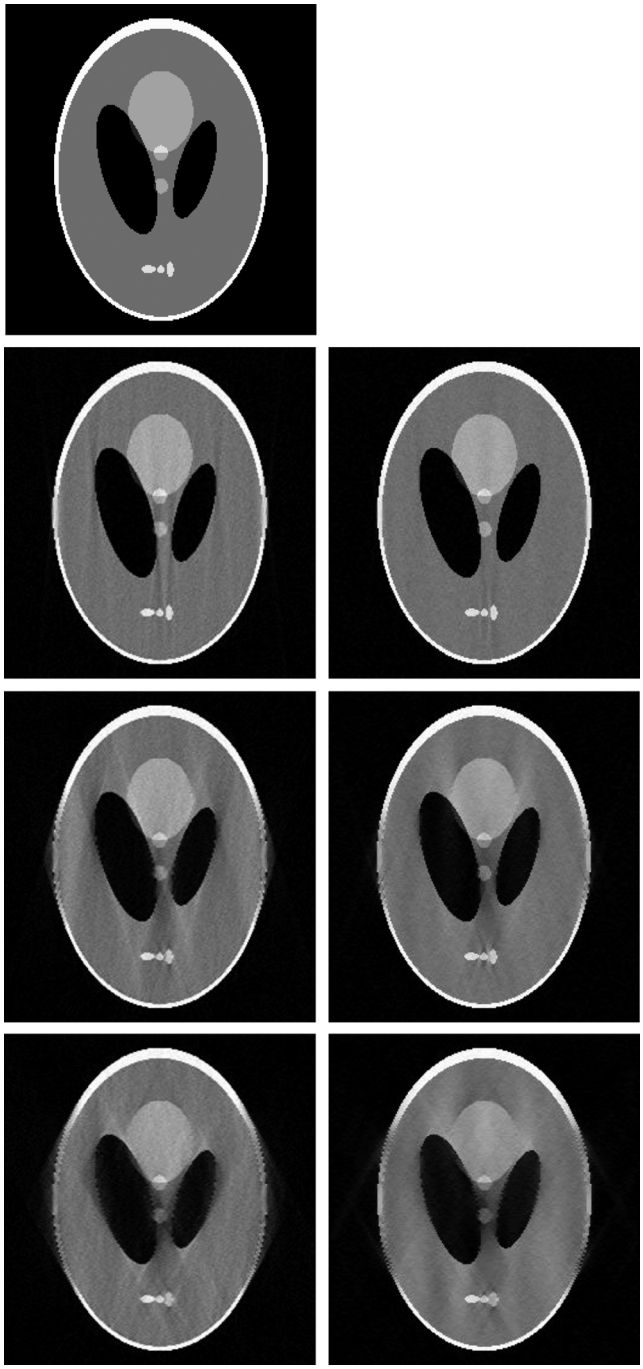

Fig. 5. Reference image (first row) and examples of the reconstructed images. Columns 1 and 2 show the images reconstructed using respectively the TV and $\delta - u$ methods. The ranges of projection angles are 166°, 142°, and 118° respectively from the second row to the last row.

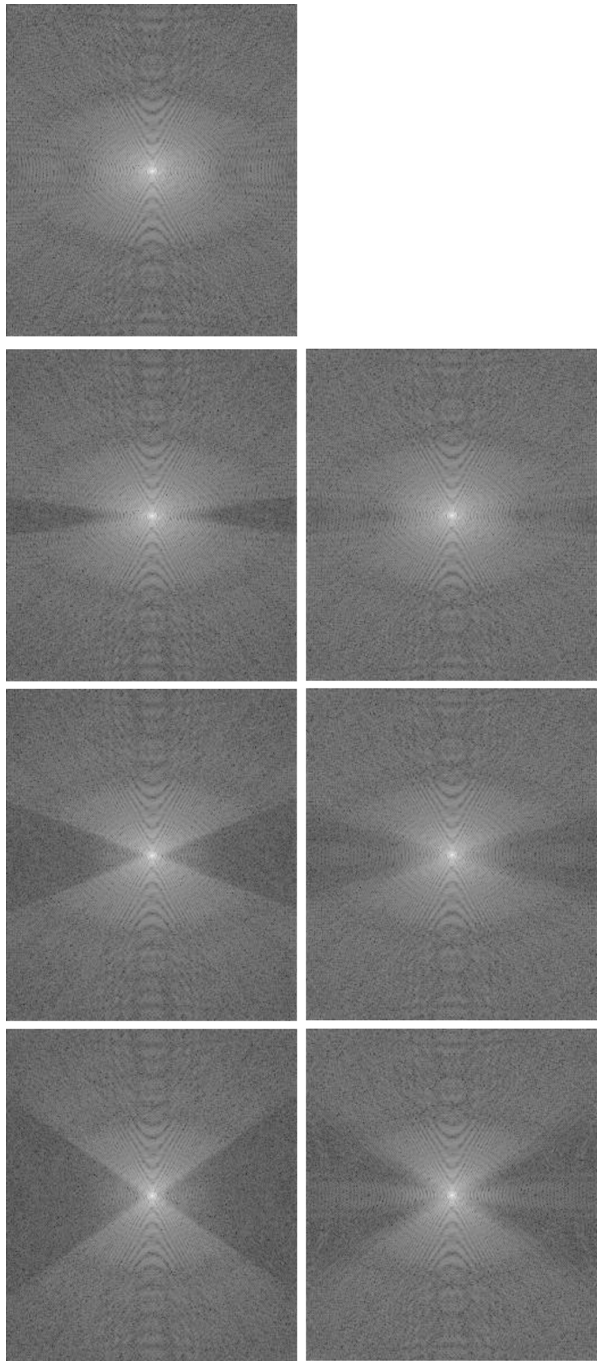

Fig. 6. Corresponding Fourier spectra of the images shown in Fig. 5.

image obtained with the proposed method is about 34.1 dB compared with 27.9 dB for the image obtained with the TV method. In addition, the reconstruction error of the proposed method decreases more quickly than that of the TV method as projection angle range increases. This means that the $\delta - u$ method can more effectively utilize the available projection data and, thus, reconstruct the image more accurately.

On the other hand, the proposed method is more sensitive to the projection angle range than the TV method. When the range of the projection angle is less than 90°, the trend of the error curves indicates that the TV method may produce better images than the $\delta - u$ method. This is probably because not all of the singular points can be extracted when the range of the projection angles is too small.

Fig. 5 shows the reference image $f_0(x, y)$ (first row) and the reconstructed images for three projection angle ranges. The projection angle ranges were 166°, 142° and 118° respectively from the second row to the last row. Images in the first and second columns are the images reconstructed respectively using the TV and $\delta - u$ methods. The corresponding Fourier spectra of the images in Fig. 5 are shown in Fig. 6. It is clear that the TV method created severe artifacts in the reconstructed images

TABLE I
PSNRs (dB) OF THE IMAGES RECONSTRUCTED BY THE TV AND $\delta - u$ METHODS AT DIFFERENT NOISE LEVELS

Noise levels	0	1	2	3	4	5	6	7	8	9
Noise STD		50.0	100.0	150.0	200.0	250.0	300.0	350.0	400.0	450.0
Projection-SNR (dB)		44.2	37.3	34.2	31.8	29.8	28.1	26.9	25.8	24.5
TV-PSNR (dB)	29.0	28.7	28.4	28.3	28.1	27.9	27.6	27.4	27.1	26.8
$\delta - u$ -PSNR (dB)	41.7	40.6	38.7	37.7	35.5	34.1	32.6	31.6	30.2	29.1

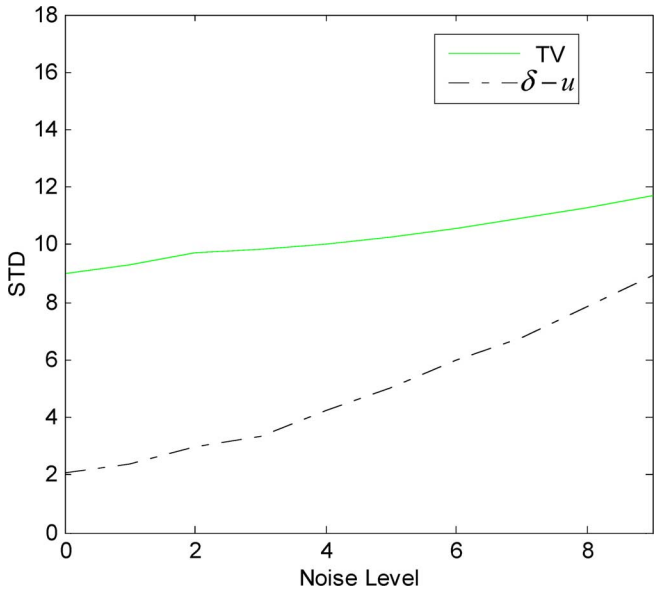

Fig. 7. STD values of the TV and $\delta - u$ methods at different noise levels when the range of the projection angles is 144°.

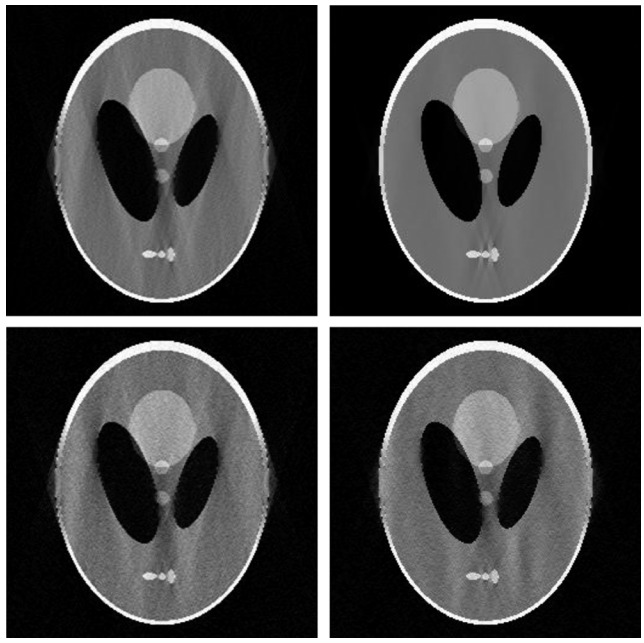

Fig. 8. Images reconstructed by the TV method (left column) and the proposed $\delta - u$ method (right column) at noise levels 1 (upper row) and 9 (lower row).

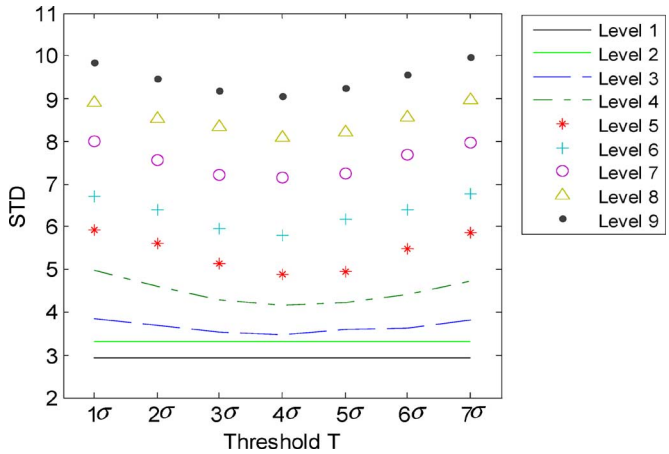

Fig. 9. Variation of the STDs of reconstruction errors as a function of threshold T used in the proposed $\delta - u$ method.

in each situation and the images produced by the $\delta - u$ method have sharp edges. From the spectra shown in Fig. 6, it can be easily seen that the TV method has little ability to reconstruct missing spectral data. In contrast, the $\delta - u$ method effectively recovered the missing spectral data. The overall texture pattern of the missing spectral data was surprisingly recovered by the $\delta - u$ method whereas the TV method was not able to recover the pattern.

We also conducted the experiments to test the noise sensitivity of the proposed $\delta - u$ method. In the experiments, zero-mean Gaussian noise was added to the projection data of Shepp–Logan head phantom. The STD values corresponding to different noise levels and the SNRs of the projection data are given in Table I. Fig. 7 shows the STD values for both the TV and the proposed methods when the projection angle range was set to 144° (scanning from 18° to 162°) and the corresponding PSNRs of the reconstructed images are given in Table I. Overall, the proposed $\delta - u$ method reconstructed the images more accurately with far lower STD and higher PSNR values than the TV method for all specified noise levels. It is interesting to notice that in the noise-free case, the PSNR of the image obtained with the proposed method reaches 41.7 dB whereas the PSNR of the image obtained with the TV method is only 29.0 dB. Obviously, the TV method failed to give desirable improvement in reconstruction accuracy in this case. Notice that the STD value for the $\delta - u$ method increases as the noise level of the projection data increases. This is mainly because noise may cause false detection of singular points. In a case when the noise level is extremely high the TV method may produce better image than the $\delta - u$ method since the noise could severely corrupt the singular points. Fig. 8 shows the images reconstructed by the TV method (left column) and the proposed $\delta - u$ method (right column) at noise levels 1 (upper row) and 9 (lower row). In both cases, the $\delta - u$ method produced sharper and more accurate images.

In the above experiments, the threshold T in the $\delta - u$ method was fixed to 4σ where σ is the standard deviation of the noise in

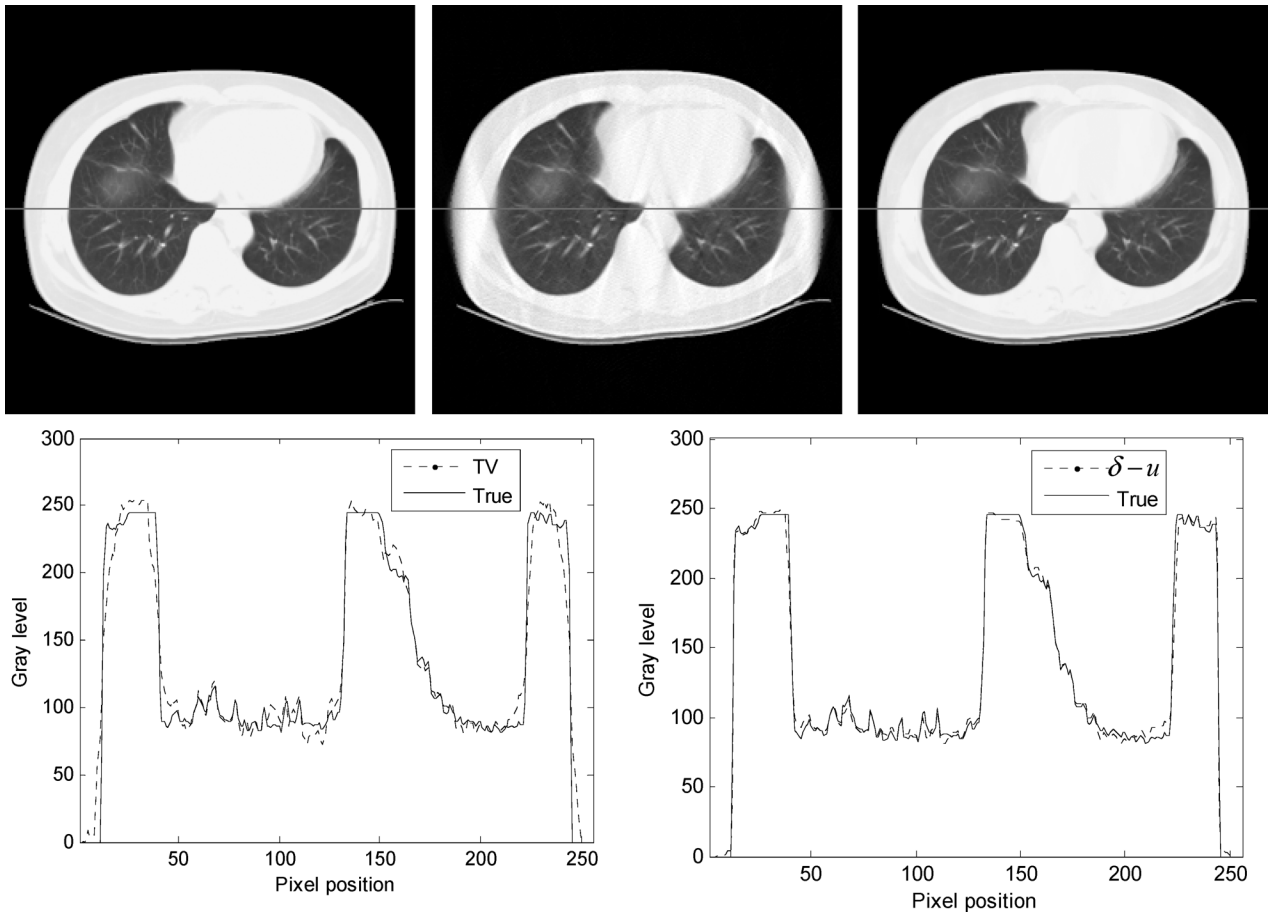

Fig. 10. Reconstructed lung CT images. Upper row: The true lung CT image (left) and the images reconstructed by the TV method (middle) and the proposed $\delta - u$ method (right). Lower row: Image profiles along the central horizontal lines obtained with the TV method (left) and the $\delta - u$ method (right). The corresponding true profiles are plotted as solid lines.

the image. Fig. 9 shows the sensitivity of the proposed method to the threshold T at different noise levels. As expected, the higher the noise level in the image, the larger the STD values or the reconstruction errors regardless of the T value. In our experiments, the reconstruction errors reached minimum when T was around 4σ for all noise levels except the noise levels 1 and 2 in which the reconstruction errors remained same for the T values ranging from 1σ to 7σ. This is probably because at noise level 1 or 2 the singular points were reliably detected with any of these T values. For the other noise levels, a T value of 4σ achieved a good compromise between false positives and false negatives in detecting the singular points. When the T value was significantly less or greater than 4σ, more false positives or false negatives occurred, respectively, hence, resulting in higher reconstruction errors.

To test the proposed method in the case of real images, we simulated the projection data from a lung CT image which contains both homogeneous and texture regions. Images were reconstructed from the projections scanning from 18° to 162°. In Fig. 10, the upper row shows the true lung CT image and the images reconstructed by the TV method and the proposed $\delta - u$ method, respectively. The lower row of Fig. 10 illustrates the image profiles along the central horizontal lines obtained with the TV method (left) and the $\delta - u$ method (right). The corresponding true profile is plotted as a solid line and overlapped onto the reconstructed profiles. As seen from the images, the reconstructed images appear visually comparable inside the cavity. However, in the homogeneous areas, the image obtained with the $\delta - u$ method is much closer to the true image than the image obtained with the TV method. In addition, the $\delta - u$ method reconstructed the texture area more accurately than the TV method. This can be clearly seen from the profiles.

It has to point out that the TV method has much higher computational cost than the proposed $\delta - u$ method. We implement both methods in Matlab. The number of iterations for the TV method was 100, and it took about 639 s to reconstruct one 256 $\times$ 256 image while the $\delta - u$ method only took about 9.5 s.

V. Conclusion

This paper presents an effective method for image reconstruction from limited-angle projections based on the sparse representation of a discrete image using $\delta - u$ functions. The parameters of the $\delta - u$ sparse representation are estimated from the limited-angle projection data. The $\delta - u$ sparse representation of the image substantially reduces the number of variables and, consequently, turns the ill-posed problem of limited-angle image reconstruction into a well-posed one. In most cases, the singular

points can be effectively detected from the limited-angle projection data by the proposed layered extraction algorithm and the singular degrees can be obtained by solving a set of linear equations in Fourier domain. However, high-level noise may corrupt weak singular points and cause false detection of singular points. It can also introduce errors in the estimation of the singular degrees even though the singular points are extracted correctly. The experimental results have shown that the proposed $\delta - u$ spectrum analysis method can recover missing spectral data more effectively than the TV method and reconstruct the image more accurately.

REFERENCES

[1] A. C. Kak and M. Slaney, *Principle of Computerized Tomography Imaging*. Philadelphia, PA: SIAM, 2001.

[2] V. Kolehmainen, M. Lassas, and S. Siltanen, "Limited data X-ray tomography using nonlinear evolution equations," *SIAM J. Sci. Comput.*, vol. 30, no. 3, pp. 1413–1429, 2007.

[3] B. P. Medoff, W. R. Brody, M. Nassi, and A. Macovski, "Iterative convolution back-projection algorithm for image reconstruction from limited data," *J. Opt. Soc. Amer.*, vol. 73, pp. 1493–1500, 1983.

[4] D. Verlaoeven, "Limited-data computed tomography algorithms for the physical sciences," *J. Appl. Opt.*, vol. 32, no. 20, pp. 3736–3754, l993.

[5] M. Bieberle and U. Hampel, "Evaluation of a limited angle scanned electron beam X-ray CT approach for two-phase pipe flows," *Meas. Sci. Technol.*, vol. 7, no. 8, pp. 2057–2065, 2006.

[6] A. L. Kesidis and N. Papamarkos, "Exact image reconstruction from a limited number of projections," *J. Vis. Commun. Image Represent.*, vol. 19, no. 5, pp. 285–298, 2008.

[7] L. Zeng, "Image reconstruction via the finite Hilbert transform of the derivative of the backprojection," *Med. Phys.*, vol. 34, no. 7, pp. 2837–2843, Jul. 2007.

[8] T. Tomitani and M. Hirasawa, "Image reconstruction from limited angle Compton camera data," *Phys. Med. Biol.*, vol. 47, no. 12, pp. 2129–2145, 2002.

[9] T. Tomitani and M. Hirasawa, "Analytical image reconstruction of cone-beam projections from limited-angle Compton camera data," *IEEE Trans. Nucl. Sci.*, vol. 50, no. 5, pp. 1602–1608, May 2003.

[10] T. Schule, C. Schnorr, and S. Weber *et al.*, "Discrete tomography by convex-concave regularization and DC programming," *Discrete Appl. Math.*, vol. 151, no. 1–3, pp. 229–243, 2005.

[11] A. H. Anderson, "Algebraic reconstruction in CT from limited view," *IEEE Trans. Med. Imag.*, vol. 8, no. 1, pp. 50–55, Jan. 1989.

[12] G. N. Vishnyakov and O. I. Mashevskaya, "Investigation of the precision of an algebraic algorithm for the reconstruction of tomograms from projections given in a limited range of angles," *Meas. Tech.*, vol. 48, no. 8, pp. 784–788, 2005.

[13] E. Y. Sidky and X. C. Pan, "Image reconstruction in circular cone-beam computed tomography by constrained, total-variation minimization," *Phys. Med. Biol.*, vol. 53, no. 17, pp. 4777–4807, 2008.

[14] E. Y. Sidky, C.-M. Kao, and X. Pan, "Accurate image reconstruction from few-views and limited angle data in divergent-beam CT," *J. X-Ray Sci. Technol.*, vol. 14, pp. 119–139, 2006.

[15] S. Weber, T. Schule, and C. Schnorr *et al.*, "A linear programming approach to limited angle 3D reconstruction from DSA," *Meth. Inf. Med.*, vol. 43, no. 4, pp. 320–326, 2004.

[16] G. T. Herman and R. Davidi, "Image reconstruction from a small number of projections," *Inv. Probl.*, vol. 24, p. 045011, 2008, 17pp.

[17] Y. H. Zhang, H. P. Chan, and B. Sahiner *et al.*, "A comparative study of limited-angle cone-beam reconstruction methods for breast tomosynthesis," *Med. Phys.*, vol. 33, no. 10, pp. 3781–3795, Oct. 2006.

[18] M. Rantala, S. Vanska, and S. Jarvenpaa *et al.*, "Wavelet-based reconstruction for limited-angle X-ray tomography," *IEEE Trans. Med. Imag.*, vol. 25, no. 2, pp. 210–217, Feb. 2006.

[19] L. Ren, J. Zhang, and D. Thongphiew *et al.*, "A novel digital tomosynthesis (DTS) reconstruction method using a deformation field map," *Med. Phys.*, vol. 35, no. 7, pp. 3110–3115, 2008.

[20] H. W. Gao, L. Zhang, Z. Q. Chen, and J. P. Chen, "Reviews of Image Reconstruction from Limited-angle," *CT Theory Appl.*, vol. 15, no. 1, pp. 46–50, 2006.

[21] M. Defrise and G. T. Gullberg, "Image reconstruction," *Phys. Med. Biol.*, vol. 51, pp. R139–R154, 2006.

Jianhua Luo was born in Zhejiang province, China, on January 9, 1958. He received the computer science M.S. degree from Hangzhou University in Hangzhou City, China, in 1992, and the biomedical engineering Ph.D. degree from Zhejiang University in 1995.

He is currently a biomedical engineering Professor with Shanghai Jiao Tong University and also served as an invited Professor at the INSA Lyon, France. He is currently principal investigator of several research projects supported by the NSFC of China and High Technology Research Development Plan (863 plan) of China. His research domain concerns magnetic resonance imaging, including image reconstruction, and image processing.

Wanqing Li (M'92) received the B.Sc. degree in physics and electronics in 1983 and the M.Sc. degree in computer science in 1987 from Zhejiang University, China, and the Ph.D. degree in electronic engineering from the University of Western Australia in 1997.

He was a Lecturer (1987–1990) and Associate Professor (1991–1992) at the Department of Computer Science, Zhejiang University, China. He joined Motorola Labs, Sydney, Australia (1998–2003), as a Senior Researcher and later as a Principal Researcher. From December 2007 to February 2008, he was a visiting researcher at Microsoft Research, Redmond, WA. He is currently with SCSSE, University of Wollongong, Australia. His research interests include medical image processing and analysis, human motion analysis, audio and visual event detection, and object recognition.

Dr. Li has served as a publication chair of MMSP'08, General Co-Chair of ASIACCS'09 and DRMTICS'05, and technical committee members of many international conferences including ICIP'03-07.

Yuemin Zhu received the B.Sc. degree in telecommunications from the Huazhong University of Science and Technology (HUST), China, in 1982, and the M.Sc. and Ph.D. degrees from the INSA (Institut National des Sciences Appliquées), Lyon, France, in 1984 and 1988, respectively. He also obtained the "Habilitation à Diriger des Recherches" in 1993.

He is a permanent Research Director of the CNRS (Centre National de la Recherche Scientifique), France. He has been appointed Honorary Professor of Shanghai Jiaotong University (SJTU), Harbin Institute of Technology (HIT), China, and Chongqing Three Gorges University, China. He is currently principal investigator of several research projects on medical imaging. His research interests include image representation, reconstruction, correction, denoising, registration, segmentation, quantification, visualization, and fusion.